Evidence for Protein Misfolding in the Presence of Nanoplastics

Oldamur Hollóczki[a,*]

[a]Mulliken Center for Theoretical Chemistry, University of Bonn, Beringstr. 4+6, D-53115 Bonn, Germany

[*]holloczki@gmail.com

May 2, 2020

The possible effect of plastic nanoparticles of waste origin on biological systems is still unclear, and could pose a severe threat. Model studies on the molecular level are urgently needed in order to help revealing interplay between these particles biological systems, and thereby to indicate the direction further research. In the present study, simulated annealing molecular dynamics was adjusted and applied to generate an array of conformations for a sample peptide oligoalanine possibly binding to polyethylene and nylon 6,6 nanoplastics. The resulting structures, with a diameter up to 5 nm, were investigated with the aid of static quantum chemical calculations. The obtained data unequivocally show that both plastic nanoparticles influence the relative stability of α-helix, β-hairpin and other conformations strongly. The polyethylene nanoparticle increases the stability of the helical foldamer. The nylon 6,6 nanoplastic offers strong plastic-peptide interactions at its surface, which make the unfolding of the peptide thermodynamically highly favorable. These results further underscore that nanoplastics can do significant, molecular level damage to living organisms via facilitating the misfolding and denaturation of proteins. Furthermore, it is apparent that plastics can have very different effects on living matter depending on their composition, hence experiments with any single kind of plastics (e.g. polystyrene) should not be considered generally valid for all nanoplastics.

Keywords: Nanoplastics, Protein folding, simulated annealing, force field, GFN2-xTB

1 Introduction

Despite all efforts in reuse and recycling, a significant portion of the worldwide annually produced 400 million tons of plastic is thrown away, resulting in a severe environmental pollution in the oceans, fresh water, and on land.[1–4] It was evidenced repeatedly that through the mechanical, chemical and biological fragmentation of plastics microscopic pieces of polymers are formed, microplastics (MPs, $d < 1$ mm) and nanoplastics (plastic nanoparticles, PNPs $d < 100$ nm), which are being distributed all over the planet.[4–21] There are estimates that through the consumption of sea salt and sea food from polluted waters, food packed in plastic, and bottled water, humans consume plastic weekly in the several grams range.[22–24] Presently, the actual risks these plastics pose to the environment and to health are mostly unknown,[25] beyond the fact that their mere occurrence is not natural in the bodies of humans and other living organisms. Even with the lack of information on the exact effects of MPs and PNPs, after several years of investigations, it has been suggested repeatedly that the exposure to PNPs and the underlying problems they trigger are probably significantly higher than those for MPs.[26,27]

Most of the corresponding experiments have been conducted directly on living animals, generally aquatic species, aiming at understanding the effects on their life cycle and on their overall health.[28–30] Although such studies bear significant importance, they may be hindered by multiple difficulties, and may thereby have shortcomings.[26,27] Firstly, the relevance of these studies has been criticized, since in the experiments the animals often need to be exposed to unrealistically high concentrations of the plastic particles to allow observing biological effects.[26,31,32] Secondly, in complex media that occur in living matter, the sheer observation of PNPs is far from trivial, since they have similar size to that of bio(macro)molecules, while their chemical composition is also not different enough.[26] Thirdly, related to the previous point, the complexity of systems that contain mixtures of biomolecules and nanomaterials at the same time often limits reproducibility. In their effort to overcome these latter three issues, Al-Sid-Cheikh et al. used a low concentration of ^{14}C-labeled plastics to track where plastics can enter the bodies of the scallop *Pecten maximus*, and was able to observe that the plastic particles can enter the blood stream and every organ of these organisms.[33] However,

even with using these rather complicated measurements it remains unclear what the fate of the plastic in the organism is (e.g. if it is digested or further fragmented), and what effects the PNPs have on the shellfish. Fourthly, synthetic routes to create PNPs have been developed only for polystyrene, and therefore all related experiments focus exclusively on this polymer. However, the chemical composition must alter the effects of the plastics, since the different polymers should offer different kinds of interactions to the molecules and materials in their immediate environment.[27]

Even with no detailed chemical or biological information on the effects of PNPs on living organisms, their sheer size suggests the mode of their action. PNPs are — per definition — by at least two orders of magnitudes smaller than individual eukaryote cells, and their size is more similar to individual biomolecules. Since these materials have been evidenced[33] to enter the blood stream and organs of organisms, it is reasonable to assume that they would alter living matter on the molecular level. Therefore, the use of molecular biological and material sciences techniques shows a distinct appeal in unveiling hitherto unknown hazards plastic wastes pose to the environment.[16,34,35] The necessity to perform such studies has been expressed in multiple articles, urging experts to provide information on the physical-chemical properties and the potential effects of these elusive materials.[16,26,27]

Theoretical chemistry and molecular modeling have become invaluable tools of physics, chemistry, and molecular biology. In a few recent papers, classical molecular dynamics (MD) simulations have been employed to explore the interactions of a variety of PNPs and biomolecular systems.[36–38] It was shown that plastics alter the structural, dynamical, and mechanical properties of phospholipid bilayers.[36,37] Since cell memranes separate the extracellular matrix and the cytosol, and they have multiple roles in metabolism, signaling, adhesion, etc., these changes may be fatal to the organism in question. In another study we demonstrated that the interplay with PNPs can affect the secondary structure of peptides. On the examples of a tryptophan zipper and an oligoalanine peptide, we found indications that while polyethylene seemed to stabilize α-helical structures, other plastics, such as nylon 6,6 stabilized other isomers, which were more β-like.[38] Since such α-to-β transformations of proteins have been found to be responsible for prion diseases (Creutzfeldt–Jakob disease,

bovine spongifom encephalopathy),[39,40] and similar structural alterations have been related to Alzheimer's disease as well,[41] the importance of these findings is apparent. In agreement, recent experimental molecular biological studies showed that proteins become denaturated in the presence of polystyrene PNPs.[42–44]

Although these results clearly show that some plastics can indeed change the secondary structure of proteins, there are certain limitations of the applied regular equilibrium MD simulations, which need to be underscored here. In MD simulations, barriers larger than a few kJ mol^{-1} cannot be overcome at room temperature. Thus, the relative populations of conformations that are very different in energy, or separated by larger barriers, cannot be obtained from these computer experiments. Furthermore, the system might stay in a metastable state due to not overcoming the activation energy to find the global minimum on the potential energy surface, which may lead to erroneous structural and energetic data. For this reason, further studies are necessary to uncover the full extent of the underlying physical chemical effects, and to quantify the changes the plastic induces in the relative stability of peptide or protein foldamers.

There are multiple approaches to tackle these issues, allowing more accurate, enhanced sampling[45–50] of complex pontential energy surfaces, including replica exchange,[51–53] meta-dynamics,[53–55] and simulated annealing (SA).[56–61] In SA, the system is simulated at a high (often physically unrealistic) temperature, which allows exploring a large portion of the conformational space. Through gradual cooling to a low temperature, the less stable conformations become depopulated, steering the system to low-lying minima, ideally to the global minimum of the potential energy surface. Although already a single simulation enables the system to visit a large number of conformations, generally multiple SA simulations are performed, in order to ensure that the global minimum is found.[60] The temperature program is often adjusted to the chemical nature of the given compound(s), in order to achieve the greatest efficiency in terms of computer time and the quality of the resulting structures.[59] This approach has been often used to generate models of solid compounds for modeling purposes, to find the global minima of systems consisting of Lennard-Jones particles,[56] and it has been applied also to predict peptide and protein structures.[58–60]

Proteins and peptides have only a handful of biologically active conformations, with a highly complex, well-defined network of various interactions, and therefore finding the relevant minima is challenging, which often requires more complex techniques than SA. PNPs are, however, polymers that are composed of a single or two kinds of monomers. These monomers offer the same kinds of interactions to the surrounding medium and to the other monomeric units within the PNP, and hence PNPs should possess a myriad of minima with very similar energies. Thus, finding one of these many relevant conformations is significantly less complicated than that for proteins, thus a simple approach, such as SA should be possible to adjust for this purpose.

In the present study, SA will be adjusted to the folding of nanoplastics and a small peptide into aggregates. The method will be then used to create an array of conformations for aggregates of selected peptide-nanoplastic systems, which can be evaluated through reliable quantum chemical methods. The present, adapted approach allows not only finding the most stable conformations of the given nanoplastic-peptide systems, but also quantifying the effects of different nanoplastics on the secondary structure of proteins.

2 Models and Methods

In the present work we considered two kinds of plastics, polyethylene (PE) and nylon 6,6 (N66). Although it is likely that in surface waters PNPs will be partially oxidized, here only pristine surfaces will be considered. In a recent study[62] it was shown that polystyrene particles with an average diameter of 31.5 μm were fragmented into $d < 1$ nm nanoparticles by Antarctic krill, which means that 97% of the surface was created within the animal. Expectedly, similar processes occur also in other animals, including humans. Assuming that these larger particles are oxidized mostly at their surface before entering the animal, it is clear that the newly created, less oxidized surfaces will get in contact with biological materials faster than it could be oxidized. Thus, at a first glance pure plastic surfaces should be generally more relevant for discussing biomolecule-PNP interactions. Nonetheless, it must be mentioned here that in a recent article, Rownczyk et al. found that some oxidation occurs

on polyethylene in marine environments not only at the surface, but even up to depths of 500-600 μm from the plastic's interface, albeit to a significantly lower extent.[18] Thus, these novel results suggest that the reasoning above has its limitations, and in future studies oxidized polymers might also be interesting to consider.

The aim was to prepare nanoparticles with diameters of 4-5 nm from single polymer chains. For these sizes, whilst being practically already relevant, even geometry optimization is available with semi-empirical quantum chemical methods. For this purpose, 16 chains of $C_{72}H_{146}$ were taken to model PE, and 8 chains of $C_{156}H_{288}N_{26}O_{27}$ for N66, the Lewis formulae are shown in Figure 1. The reason behind selecting fewer and longer chains for N66 than for PE was to allow several of the (longer) monomer units to repeat in a single polymer molecule, and thereby avoid having proportionally too many terminal monomer moieties, while also maintaining the overall size of the particle. To model the interaction of these PNPs with proteins, a model peptide oligoalanine was chosen, composed of twelve alanine units (Ala_{12}, Figure 1). This molecule was considered in two conformations, once in an α-helical and once in a β-hairpin conformation (Figure 2). The generation of the latter species, as well as further conformations will be described in detail in the next chapter.

Classical molecular dynamics simulations were performed by using the Lammps program.[63] The potential energy was estimated through the OPLS-AA force field.[64] The cutoff for intermolecular interactions was chosen to be 10 Å, beyond which Coulombic interactions were estimated through the particle-particle particle-mesh method. The timestep was 1 fs in all simulations. To control the temperature, the Nosé–Hoover thermostat was used, with a time constant of 100 fs. The rest of the settings for the MD simulations had to be optimized in the present work, and therefore they will be described in the next chapter. After all simulations, the resulting structure was optimized through the Polak–Ribiere version of the conjugate gradient (CG) algorithm, with a convergence criterion of 10^{-6} for the change in energy (unitless value for the ratio of the energy change divided by the energy magnitude), and $10^{-7}\,\mathrm{g\,Å\,mol\,fs^{-2}}$ for the forces. Thereafter, another minimization was performed through the Hessian-free truncated Newton (HFTN) algorithm, with convergence criteria 10^{-8} for the energy, and $10^{-8}\,\mathrm{g\,Å\,mol\,fs^{-2}}$ for the forces. If either of the two criteria were met, the

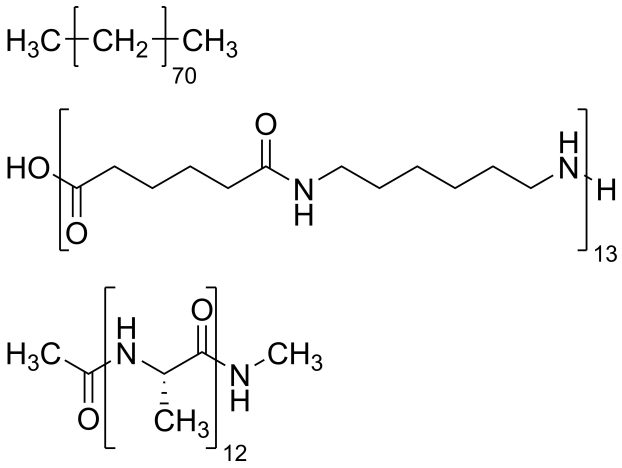

Figure 1: Lewis structure of the molecules investigated in the present article: The polyethylene model $C_{72}H_{146}$ (doheptacontane, above), the nylon 6,6 model $C_{156}H_{288}N_{26}O_{27}$ (middle), and oligoalanine Ala_{12} (below).

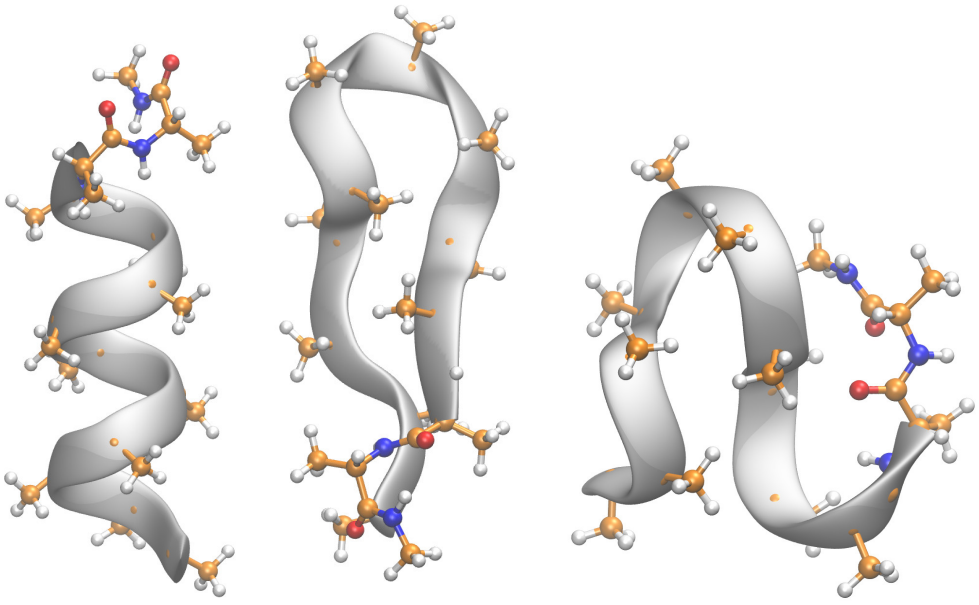

Figure 2: Ball-and-stick representation of the α-helix (left) and β-hairpin conformation of the investigated oligoalanine model peptide (middle). The most stable not helical or β-hairpin-like conformation of the peptide, obtained through simulated annealing in the gas phase, is also shown (right).

optimization was considered converged. Finally, single point energy was calculated with the cutoff distance increased to 60 Å. The development of interatomic distances in the trajectories was obtained by using the Travis code.[65,66]

For the obtained systems, having up to 4108 atoms, semi-empirical extended tight-binding GFN2-xTB calculations were performed by the xtb program package.[67,68] Using a minimal valence basis set, GFN2-xTB is based on a DFTB3-like scheme, including electrostatic interactions, exchange-correlation effects up to the second order in the multipole expansion, without relying on any element pair-specific parameters. Most importantly, this method incorporates the D4 dispersion correction as well,[69,70] hence for the systems investigated here — presumably governed by weak, dispersion interactions — it exhibits a direct appeal. For non-covalent interactions and conformational energies, GFN2-xTB showed less than a few kcal mol^{-1} mean absolute deviation from various benchmark sets, outperforming many GGA and hybrid functionals.[68] Furthermore, it was recently shown that for the structure and energetics of proteins GFN2-xTB provides very accurate quantum chemical data,[71] which makes this method even more promising for the present purposes. The energy convergence for the SCF was set to 10^{-6} Eh. Geometry optimizations were performed with the FIRE algorithm, in which the "normal" convergence settings were applied, with a $5 \cdot 10^{-6}$ Eh for the energy, and 10^{-3} Eh α^{-1} for the gradient. For convergence, both criteria had to be met. To model the water solvent, the GBSA implicit solvent model with "tight" settings for the grid were chosen. The energy quantities that were used to characterize the PNP-peptide interactions in the following chapter are defined in Figure 3.

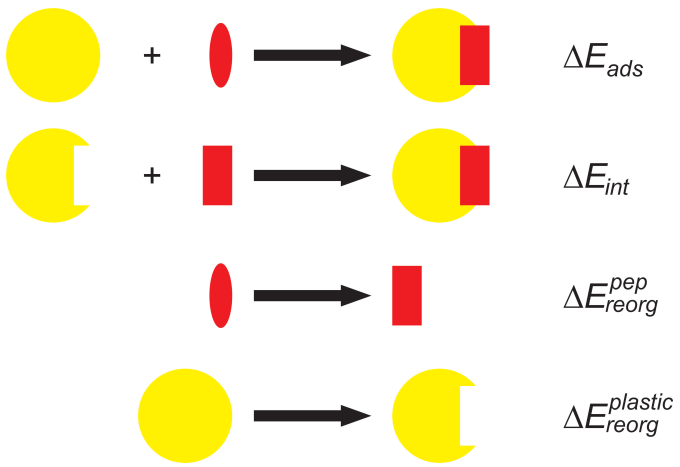

Figure 3: Definition of the energy quantities that are used in the article to characterize the PNP-peptide interaction. The plastic particle (yellow) and the peptide (red) both suffer conformational changes in the complex formation (top row), which can be quantified through the reorganization energies $\Delta E_{reorg}^{plastic}$ and ΔE_{reorg}^{pep}, respectively. If the overall adsorption energy (ΔE_{ads}) is to be a negative value, these must be compensated by a high interaction energy (ΔE_{int}) in these altered conformations.

3 Results and Discussion

3.1 Optimizing Simulated Annealing to Nanoplastic-Protein Systems

Simulated annealing (SA) was started at high temperatures, at which the polymer chains that constitute the PNP studied here can stay dissociated, and move through space independently with a high kinetic energy. To facilitate the condensation of these individual macromolecules into a single particle, periodic boundary conditions were applied, prohibiting the chains to diffuse too far from each other in space. The cell vector of the cubic simulation boxes were chosen to be 150 Å, which is long enough to avoid the chains interacting with their own images, even if they are fully in a linear arrangement, with *trans* conformations for all C-C-C-C units.

The initial test has been performed for polyethylene in a single molecular dynamics simulation, in which the system was equilibrated for 1 ns at 750 K, and then cooled to 200 K over a 10 ns production simulation in a linear temperature program (Figure 4). To track the development of the structure, two quantities are introduced here. The first one was chosen to quantify how much the molecules spread radially in space, thus, the progress of forming a single nanoparticle. Generally, moment of inertia

$$I_a = \sum_i m_i r_{i,a}^2 \tag{1}$$

is a quantity that represents well the radial extent of a system, where m_i is the mass of mass point i, and $r_{i,a}$ is the distance of this mass point from the rotational axis a. Since in this case rotation is irrelevant, this quantity was slightly modified to the axis-independent

$$I = \sum_i M_i r_i^2, \tag{2}$$

where M_i is the relative atomic mass of atom i, and r_i is its distance to the center of mass of the whole system. The other relevant quantity should represent the rearrangement of the molecules within that particle, viz. their mobility. For this purpose, the intramolecular distances between the terminal carbon atoms of each chain were selected (R). This quantity clearly shows if the molecules are mobile, and if they explore multiple conformations during the simulations.

The developemnt of I shows that the system is dispersed at higher temperatures, but starts a partial condensation at around 500 K. Upon further cooling, at about 400 K, I drops to a lower value, and remains in the same magnitude through the rest of the simulation. Thus, the condensation of the macromolecules into a single nanoparticle occurs at this point. Visual inspection of the structures supports this conclusion. Turning to R, it is visible in Figure 4 that the intramolecular distances between the terminal carbon atoms of the polyethylene molecules fluctuate in a wide range, inferring fast changes in the chain conformations. At the condensation temperature, R drops to a low value, showing that these long alkanes assume

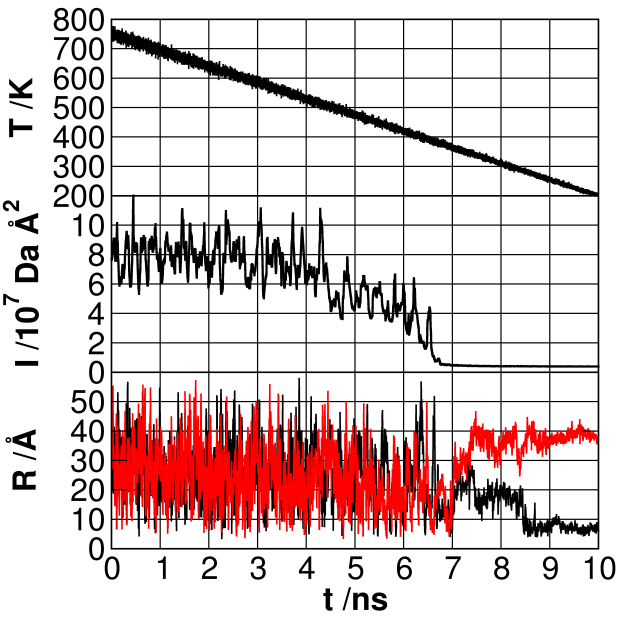

Figure 4: Development of the temperature (T, above), and the structure of 16 $C_{72}H_{146}$ chains in a simulation box over the 10 ns molecular dynamics simulation. The moment of inertia-like quantity I is defined according to Eq. 2, and characterizes the spatial extent of the system (I, middle). The development of intramolecular distances between the terminal carbon atoms of two selected chains shows the mobility of the molecules in the system, and the changes in their capacity to rearrange as the temperature is decreasing (R, below).

a hairpin-like structure just before completing aggregation. Thus, initially, the nanoparticle consists of loosely associated clumps of macromolecules, which are not entangled. Despite the condensation, the chains do not lose their mobility, and they slowly rearrange, exhibiting varying R values. Due to this movement, over the course of the simulation the chains intertwine, and a fully entangled nanoparticle emerges. Finally, at about 250 K the mobility of the macromolecules diminishes, and the particle freezes.

Thus, the PNP explores three phases upon cooling: above ca. 400 K it is a vapor, below 250 K it is a solid, while in between it behaves as a liquid nanodroplet. The experimental melting and vaporization points of $C_{72}H_{146}$ (doheptacontane) are 379.5 K and 923.94 K, respectively. The difference between the experimental values, and the present results can be rationalized through the limited size of this particle, as 16 molecules should not exhibit bulk

behavior. Nanoparticles and nanodroplets are known to have very different phsyical properties compared to the liquid or solid state of the same material, for instance a significantly higher vapor pressure, which is in line with the observed differences. For finding the lowest energy minima on the potential energy surface, it is reasonable to assume that the liquid phase is of high importance, since in the solid phase the molecules or the particle do not have the necessary mobility to shift from one conformation to another, whereas the gas phase is just structurally too different from the conformations that are aimed at here. Therefore, it can be hypothesized that the efficiency of the SA approach is highly dependent on how long the liquid plastic nanodroplet is simulated. Considering the development of I and R in Figure 5 defines an ideal upper and lower temperature limit for the SA, being at or slightly above the condensation point, and at or slightly below the freezing point, respectively.

To test this hypothesis, a series of test simulations were performed. First a set of ten input structures were created from an initial 10 ns molecular dynamics simulation run of the system at 750 K, where the geometry was saved after every ns. SA was performed on each of these structures, with three varying parameters: the starting highest temperature (T_{start}, from which the cooling program starts), the lowest temperature (T_{end}, defining the target temperature for the cooling), and the length of the simulation (t_{run}, defining a rate of cooling). The default parameters were $T_{start} = 550\,\mathrm{K}$, $T_{end} = 200\,\mathrm{K}$, and $t_{run} = 10\,\mathrm{ns}$, from which two were kept constant, while the third was altered through a wide range. Every MD simulation was concluded with a rigorous energy minimization procedure, as described in the methodology section. The resulting relative potential energies are shown in Figure 5.

The changes in the relative potential energies show that the choice of the parameters is paramount for the production of stable conformations. According to the data, and in agreement with the discussion above, T_{start} should be chosen to be around the point, where the condensation begins, in this case at ca. $T_{start} = 400\,\mathrm{K}$. The length of the run is also an important factor, since it should leave enough time for larger structural reorganization. For small proteins SA has been shown to be efficient already with simulations shorter than 100 ps.[60] In contrast, for the present, larger aggregate 1 ns is still insufficient, and the potential energies seem to converge only if the cooling program is conducted at least through $t_{run} = 20\,\mathrm{ns}$. It

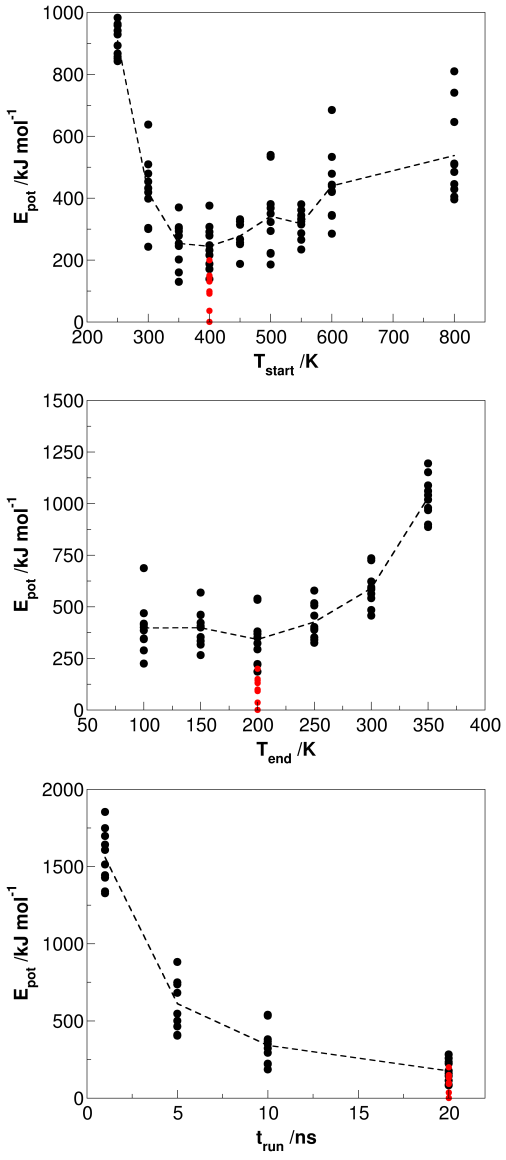

Figure 5: OPLS-AA relative potential energies of the polyethylene nanoparticles obtained at different T_{start} (top), T_{end} (middle) and t_{run} (bottom) for ten separate starting structures. In the simulations only one parameter was altered from the default $T_{start} = 550\,\mathrm{K}$, $T_{end} = 200\,\mathrm{K}$ and $t_{run} = 10\,\mathrm{ns}$ settings. The dashed lines connect the average values obtained for each setting. The red points show the potential energies for the optimized $T_{start} = 400\,\mathrm{K}$, $T_{end} = 200\,\mathrm{K}$ and $t_{run} = 20\,\mathrm{ns}$ setup.

is apparently also important to cool the system to low temperatures, although cooling below $t_{run} = 200\,\mathrm{K}$ is apparently unnecessary, and instead it increases the cooling rate, rendering

the corresponding SA settings somewhat less efficient.

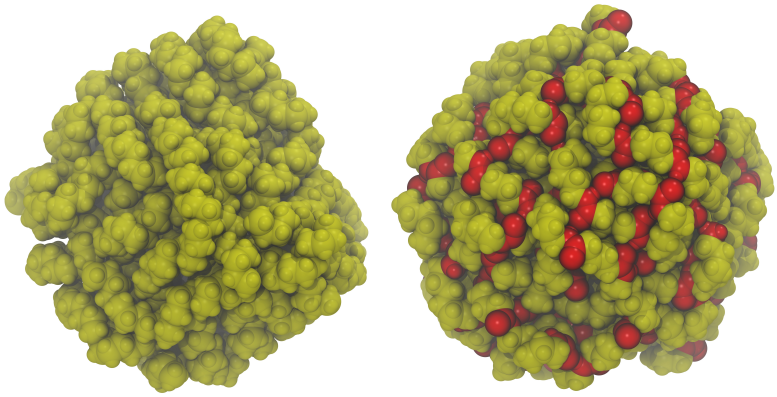

Figure 6: The structure of the most stable polyethylene (left) and nylon 6,6 (right) nanoparticles. The polar amide moieties of the nylon particle are colored red, revealing the chains of hydrogen bonds that span through the whole nanoparticle.

In the lowest energy geometry (Figure 6 left), the chains assemble as expected, aligning parallel to each other, and form a spherical nanoparticle. Next to the several sections with the expected dominance of the *trans* C-C-C-C conformations, *gauche* configurations appear, resulting in numerous turns and hairpins (Figure 7 left). While this structure looks counterintuitive given that the OPLS-AA dihedral parameters set a clear preference for the trans structures, these units are necessary for coiling the chains into a highly stable, spherical shape. Apparently, the energy gain from the stabilizing van der Waals interactions in the more compact structures overcomes the energy penalty for the *gauche* conformations.

The nylon 6,6 chains are fundamentally different from polyethylene in terms of their interplay with their environment. Whilst polyethylene is non-polar, and the interactions between the chains are exclusively through weak dispersion interactions, nylon 6,6 possesses amide moieties, which — similarly to peptides and proteins — can form hydrogen bonds as well. Since hydrogen bonds are generally stronger than van der Waals interactions, the dissociation/condensation temperature as well as the freezing point is expected to be significantly higher than for polyethylene. According to the development of I in a single test simulation with $T_{start} = 1200\,\mathrm{K}$, $T_{end} = 200\,\mathrm{K}$, $t_{run} = 10\,\mathrm{ns}$, the condensation temperature is as high as 800 K. Thus, large ranges of T_{start} (300, 400, 500, 600, 700, 800, 900, and 1000 K), T_{end} (200,

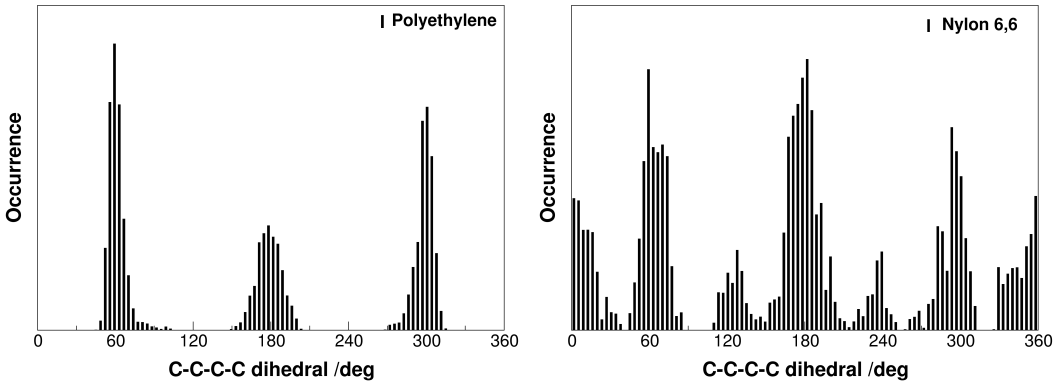

Figure 7: Distribution of C-C-C-C dihedral angles in the most stable polyethylene (left) and nylon 6,6 (right) plastic nanoparticles after geometry optimization.

300, 400, and 500 K), and t_{run} (1, 5, 10, 20, and 30 ns) were tested (see Supp. Inf.), similarly to the procedure for polyethylene above. The optimal settings chosen for the SA were found to be $T_{start} = 800\,\mathrm{K}$, $T_{end} = 200\,\mathrm{K}$, $t_{run} = 20\,\mathrm{ns}$ (see Supp. Inf.), which were again possible to deduce from the I and R values, analogously to PE.

In the most stable nylon 6,6 PNP, many chains run in a largely parallel fashion within the particle, in which their C-C-C-C units are more prevalent in *trans* conformation (Figure 7 right) than discussed for polyethylene above. Nonetheless, the dihedrals show a much higher diversity than for the other plastic, indicating again that other structural features are energetically more important than the C-C-C-C conformations. The possibility of the chains to form hydrogen bonds with each other has a distinct effect on the structure: The amide units form long chains of hydrogen bonds that span through the whole particle (Figure 6 right). The 224 hydrogen bond donor and acceptor sites in the system form altogether 185 hydrogen bonds. This high occupancy of hydrogen bonding sites is surprising for multiple reasons. Firstly, hydrogen bonding sites are separated by six carbon atoms, therefore a highly ordered alignment has to be reached by the SA. Secondly, the small size of the particle, and the resulting curvature also imposes a certain structure on the macromolecules, if it is to be relatively spherical. Compactness and hydrogen bonding should therefore compete in determining the conformation. Thirdly, not unrelated to the previous point, the

small size of the PNP should limit the length of hydrogen bonding networks, resulting in several unoccupied end groups. Despite these effects, not only an extensive hydrogen bonding network is created, but the individual chains of hydrogen bonds are also ordered with respect to each other spatially into parallel stripes of polar groups (Figure 6 right), creating polar and non-polar microstructures within the PNP. The hydrogen bonds are formed not with the neighboring amide units intramolecularly, but between different chains, or at least more distant groups of the same chain, and thereby a rough β-sheet-like structure emerges (Figure 6). The spontaneous formation of these complex structural features shows how powerful SA is for studying the structure of PNPs.

3.2 Interactions of Plastic Nanoparticles with a Peptide

The protein model considered in the present study was an oligoalanine peptide, containing 12 alanine units, and amide functionalities closing the terminal positions, as shown in Figures 1 and 2. The two conformations that were first considered are the α-helix (Figure 2 left), and the β-hairpin (Figure 2 right). Generally, structurally stable β-sheets are significantly larger peptides, and small β-hairpins are difficult to design. Thus, for defining the β-hairpin foldamer of the Ala_{12} oligoalanine, the geometry of the backbone of a previously characterized β-hairpin, a tryptophan zipper (PDB ID: 1LE1)[72] was taken as a template, which — similarly to Ala_{12} — contained twelve amino acid units. The helical and hairpin structures were both optimized with the GFN2-xTB method, yielding a relative energy of 92.9 kJ mol^{-1} for the β-hairpin with respect to the α-helix (Table 1). The structures were reoptimized employing the generalized Born model with hydrophobic solvent accessible surface area (GBSA) implicit solvation model to account for the interactions with aqueous solution. In the presence of the water solvent, the relative energy of the β-hairpin increases to 136.1 kJ mol^{-1} (Table 1).

Further conformations of the peptide were created by simulated annealing. Among the helical and β-hairpin-like structures, numerous conformations were obtained that cannot fit in either of these two categories. Optimized at the GFN2-xTB level, these geometries are somewhat globular, with several intramolecular hydrogen bonds (Figure 2 right). Presumably due

Table 1: GFN2-xTB relative energy of the most stable α-helix, β-hairpin, and unordered structures in the presence and absence of polyethylene (PE) or nylon 6,6 (N66) plastic nanoparticles, in the gas phase, and in aqueous solution. Adsorption energies (ΔE_{ads}) are also shown (with respect to the corresponding most stable free peptide in an analogous conformation, and the most stable free plastic nanoparticle), together with the plastic-peptide interaction energy within the complex (ΔE_{int}), and the reorganization energy of the plastic particle ($\Delta E^{plastic}_{reorg}$) and the peptide ($\Delta E^{pep}_{reorg}$). For the definition of the quantities, see Figure 3.

Peptide conf.	Plastic	Solvent	ΔE_{rel} kJ mol^{-1}	ΔE_{ads} kJ mol^{-1}	ΔE_{int} kJ mol^{-1}	ΔE^{pep}_{reorg} kJ mol^{-1}	$\Delta E^{plastic}_{reorg}$ kJ mol^{-1}
α-helix	–	–	0.0	–	–	–	–
β-hairpin	–	–	73.1	–	–	–	–
unord.	–	–	7.5	–	–	–	–
α-helix	–	water	0.0	–	–	–	–
β-hairpin	–	water	136.1	–	–	–	–
unord.	–	water	65.8	–	–	–	–
α-helix	PE	–	0.0	−211.7	−314.8	10.3	92.8
β-hairpin	PE	–	132.4	−152.4	−174.7	2.1	20.2
unord.	PE	–	60.2	−159.0	−248.2	58.7	30.4
α-helix	PE	water	0.0	−133.3	−201.5	5.7	62.6
β-hairpin	PE	water	175.3	−94.1	−117.4	3.3	20.0
unord.	PE	water	108.5	−90.5	−155.7	52.6	12.6
α-helix	N66	–	0.0	96.6	−445.0	24.0	517.6
β-hairpin	N66	–	116.1	139.6	−492.3	46.6	585.4
unord.	N66	–	−316.3	−227.2	−800.4	256.8	316.3
α-helix	N66	water	0.0	169.8	−271.8	17.5	424.1
β-hairpin	N66	water	75.2	108.9	−353.0	40.0	421.8
unord.	N66	water	−256.4	−152.4	−576.2	209.8	214.1

to these latter interactions, the most stable of these conformations have very low relative energies, only 7.5 kJ mol^{-1} above the α-helix in the gas phase (Table 1). In aqueous solution the relative energy of this structure increases to 65.8 kJ mol^{-1}.

After obtaining the ideal SA procedure for creating the PNPs, the focus was shifted onto folding the plastic together with a peptide. The optimization procedure for the SA could be performed anew for these mixtures of materials, however, since the plastic constitutes the overwhelmingly larger portion of these systems, it is reasonable to assume that the physical chemical properties of the plastic determine the folding process. For this reason, the condensation temperature of the plastic-peptide mixture should be similar to that of the neat plastic, hence these SA simulations were also performed with the settings established above.

For each peptide-plastic mixture, altogether 150 SA runs were performed. It is conceivable that the plastic condenses around the peptide, and thereby freezes it into an unfavorable conformation that cannot rearrange through cooling. To ensure the availability of all characteristic conformations of the peptide on (or within) the plastic, the aforementioned 150 simulations were separated into three groups. In the first group of 50 simulations, the α-helix conformation of the peptide (Figure 2 left) was enforced, not allowing any changes in the interatomic distances within this molecule. In the second group of 50 simulations, the β-hairpin isomer of this peptide (Figure 2 middle) was kept rigid. In the third group of 50 simulations, the peptide was allowed to freely change its conformation, similarly to the polymer chains. In these cases, the peptide showed facile conformational rearrangements at the higher temperatures of the SA simulations, changing its secondary structure from the input geometry. The latter group of simulations will be termed in the article — to indicate that the peptide can completely lose its ordered structure — *unordered* or *unord*.

In the final geometry optimization of each system by the force field, all constraints were lifted. On the resulting structures, GFN2-xTB single point calculations were performed, and on those that were in the lowest 25 kJ mol^{-1} in quantum chemically obtained energy in each group of 50 structures, geometry optimizations were carried out. The single point energy calculations, selection of most stable structures, and the subsequent geometry optimizations

were repeated using the GBSA solvent model to account for the aqueous medium. In the article only the most stable one of the obtained optimized structures of each group will be discussed. The resulting energetic data are compiled in Table 1.

The systems containing the polyethylene chains and the peptide show a high structural diversity, with varying location and orientation of the latter species. In the most stable structure with the α-helix isomer (Figure 8 top), regardless of the solvation model, the oligoalanine is encompassed by the PE chains, only a fraction of it is exposed to the surrounding solvent. This finding is a good agreement with earlier molecular dynamics simulations,[38] in which we found that the PE molecules rearrange upon contact with the peptide, giving way to the peptide to penetrate the PNP. In contrast, the β-hairpin conformer is apparently excluded from the PNP, and it remains at the surface of the particle (Figure 8 middle). In the last group of simulations with the free movement of the peptide, the peptide conformations show a significant variation, including some partially helical, or hairpin-like structures as well. The most stable conformation (Figure 8 bottom), however, did not resemble either of the two aforementioned secondary structures, it showed a rather compact, globular geometry, strongly resembling the structure of the neat peptide obtained through SA (Figure 2 right). The peptide in this conformation also penetrates the plastic, and covered by a single chain of the polyethylene. Nonetheless, the encompassment in this case is significantly less pronounced than for the α-helix foldamer (Table 1).

Gas and aqueous phase adsorption energies (ΔE_{ads}, see Figure 3) are in all cases negative, indicating that regardless of conformation the peptide is prone to interact with the nonpolar PE-PNP (Table 1). For all conformations, the presence of the water solvent makes the ΔE_{ads} values by ca. 60-80 kJ mol^{-1} less negative, due to the solvation of the peptide. The adsorption energies are highest for the helical structures, followed by the other two isomers with similar energies.

Dissecting these adsorption energies, the interaction energy (ΔE_{int}, see Figure 3), and the reorganization energy of the two components can be defined (ΔE^{pep}_{reorg} and $\Delta E^{plastic}_{reorg}$, see Figure 3). The interaction energy is by far highest for the α-helix, followed by the unordered structure, with the β-hairpin showing the smallest ΔE_{int} values. Since the plastic chains

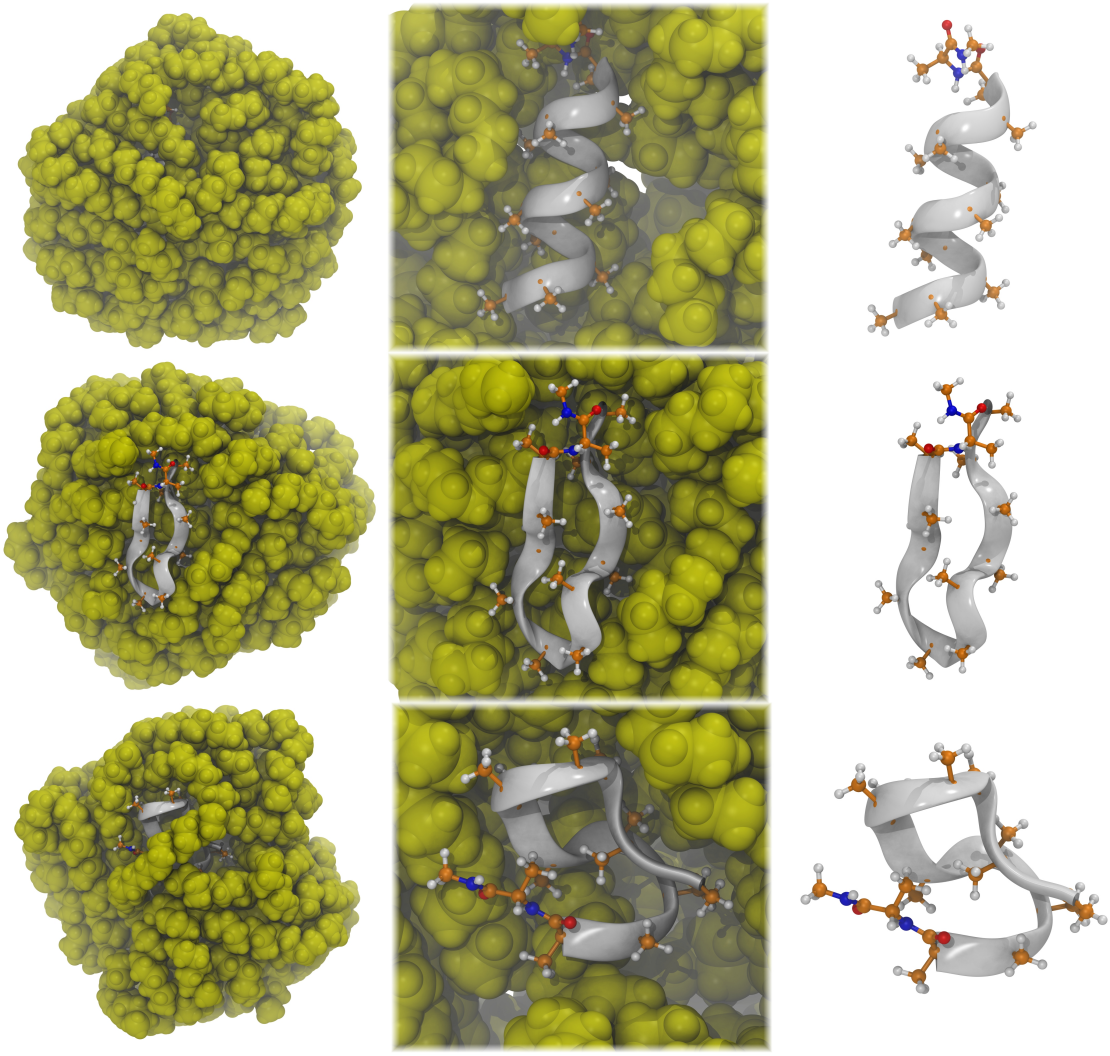

Figure 8: Most stable relevant structures for the Ala_{12} peptide at the polyethylene nanoparticle (in yellow), and the peptide (grey ribbon and ball-and-stick with blue for N, red for O, orange for C, and white for H atoms), as obtained from simulated annealing and the subsequent GFN2-xTB geometry optimization. Top: with an α-helical peptide conformation, middle: with a β-hairpin peptide conformation, bottom: with the unconstrained peptide, folded together with the plastic in the corresponding simulated annealing runs. The middle column shows the orientation of the peptide in between the polymer chains, with the interfacial chains omitted for visibility. In the right column the plastic is fully omitted, showing only the peptide.

form a pocket for the peptide within the PNP in case of the helical peptide, the plastic chains have to rearrange much more than for the other two structures, in which the oligoalanine remains more at the interface. Accordingly, the $\Delta E_{reorg}^{plastic}$ values are higher for the α-helical structures, than those for the most stable β-hairpin conformers, and the unordered peptide (Table 1). The complexes containing the α-helix and β-hairpin were created with constrained geometry for the peptide. Accordingly, the ΔE_{reorg}^{pep} values are low, which is the result of the SA procedure being performed with a constrained structure. In case of the simulations with the unconstrained peptide structure, the ΔE_{reorg}^{pep} is somewhat higher for the peptide, amounting up to 50-60 kJ mol^{-1} for the gas and aqueous phase (Table 1).

The higher ΔE_{ads} and ΔE_{int} values being accompanied by higher $\Delta E_{reorg}^{plastic}$ have an additional aspect, which is worth mentioning. This roughly opposite trend of these quantities show that the energy of the polyethylene components is not the determining factor of the relative energies, and instead it is rather the peptide-plastic interaction that is the most influential component. Therefore, the relative energies of the peptide conformations are probably not just an artifact of the faulty folding of the polymer, suggesting that the SA approach applied in this manner is an efficient and robust technique for the present purposes.

Since the adsorption energies are the highest for the α-helix conformer, the stability of this structure over the other two is further increased by the presence of the plastic. This extra stabilization by the nanoparticle amounts to about 60 kJ mol^{-1} in the gas phase, and 40 kJ mol^{-1} in the aqueous solution. In other words, the helix propensity of alanine is influenced, that is, increased by the polyethylene nanoparticle. Such a change can affect the folding of peptides through changing their secondary structure. Furthermore, the apparent capacity of the PNP to absorb the Ala_{12} α-helix but not the β-hairpin structure indicates a certain selectivity. Upon adsorption onto the surface of these nanoparticles, the polymer chains may surround fragments of a protein selectively, which would apply force on its structure, and would thereby distort its tertiary structure as well.

Nylon 6,6 differs from polyethylene in terms of the interactions it can offer the peptide. As detailed above, the N66 PNP shows a distinct hydrogen bonding network with its amide moieties, which defines a spatially ordered separation of polar and non-polar domains of

the polymer chains. The possible amide-amide interactions between the N66 PNP and the peptide, in fact, make the plastic-peptide interplay somewhat similar to protein-protein interactions. Thus, the effect of the N66 PNP on the peptide is expected to be not only stronger, but structurally more influential than that with the PE PNP. It is feasible that through incorporating the peptide into this nanostructure either the N66 PNP imposes its domain structure onto the peptide, or the peptide locally perturbs the hydrogen bond network and domain separation of the PNP. Furthermore, it is important to keep in mind that the presence of hydrogen bonding sites at the surface of the N66 also results in a high solvation energy of the PNP in water (c.f. $\Delta G_{solv} = -108.8$ kJ mol^{-1} for the PE PNP and -2215.5 kJ mol^{-1} for N66 PNP), which might counteract the adsorption of the peptide onto the surface of the plastic particle to some degree.

Among the various structures obtained with the α-helix conformation of Ala_{12}, those with the peptide at the surface of the N66 PNP were found to be the most stable. The plasic chains are oriented in a manner that they form a shallow depression at the PNP surface, which allows the partial penetration of the peptide (Figure 9 top). However, interestingly, instead of interacting with the polar moieties of the peptide, the amide groups of N66 form hydrogen bonds only with each other. The only exceptions are the terminal amide units of the peptide, which form altogether three hydrogen bonds with the plastic. Instead, the non-polar CH_2 units of the nylon can be found in the close proximity of the helix, allowing the weaker, dispersion interactions to dominate the plastic-peptide interplay (Figure 9 top). This finding is in good agreement with the affinity of this helical species to interact with non-polar chains, as described above for the PE PNP. The spatial rearrangement of the N66 chains, which allow incorporating the Ala_{12} into the particle, induces a gap into the PNP structure. This change disturbs the hydrogen bonding network between the polymer units, which is well-represented by the decrease of the total number of hydrogen bonds from 185 in the neat PNP to 161 in the presence of the peptide.

In the most stable structure obtained containing a β-hairpin foldamer of the Ala_{12}, the peptide is partly enclosed between the chains of the PNP, presenting only a part of its surface to the solvent (Figure 9 middle). This β-sheet analogue is less compact than the

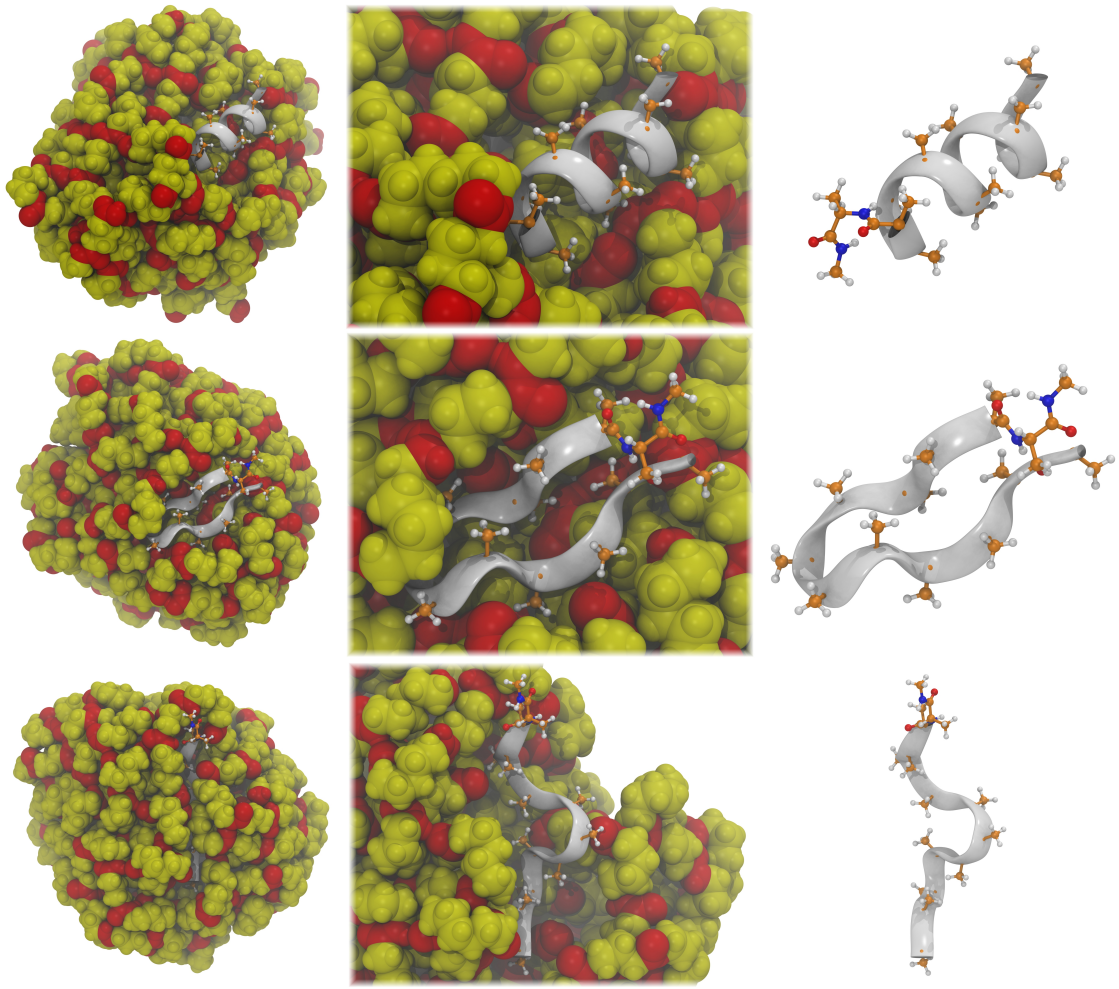

Figure 9: Most stable relevant structures for the Ala_{12} peptide at the nylon 6,6 nanoparticle (carbon atoms an non-polar hydrogen atoms are yellow, N-H groups and oxygen atoms are red), and the peptide (grey ribbon and ball-and-stick with blue for N, red for O, orange for C, and white for H atoms), obtained from simulated annealing. Left: with an α-helical peptide conformation, middle: with a β-hairpin peptide conformation, right: with the unconstrained peptide, folded together with the plastic in the corresponding simulated annealing runs.

helix, presenting half of its oxygen atoms and half of its N-H hydrogen atoms to the adjacent molecules. Many of these hydrogen bonding sites are accompanied by their counterparts at the plastic surface, resulting in nine hydrogen bonding interactions between the PNP and Ala_{12}. In return, however, the plastic loses several hydrogen bonds compared to the neat structure, leaving only 167 of them intact. This decrease in the number of hydrogen

bonds is smaller than that for the helical isomer, and the nine peptide-PNP hydrogen bonds compensate more effectively for the corresponding destabilization. Nonetheless, the total number of hydrogen bonds in the system is still smaller than that for the separated neat plastic and peptide combined. This finding, and the enclosed situation of the peptide suggests that the presence of this isomer of the peptide disrupts the structure of the N66 PNP.

The unordered peptide is adsorbed onto the N66 PNP as an almost fully linear, open chain, which is largely covered by the neighboring moieties of the N66 macromolecules (Figure 9 below). The middle section of the peptide features a small loop. The two sides of this loop run, however, parallel to each other, forming no intramolecular hydrogen bonds with each other. Many hydrogen bonding sites of the Ala_{12} are matched by the plastic surface, resulting in altogether nine N-H$\cdots$O hydrogen bonds between the nylon particle and the peptide. This severe change in the structure of the unordered peptide compared to that in the absence of any plastics or in the presence of the PE PNP suggests that its geometry is largely adjusted to the PNP, leaving the nanostructure of the plastic more intact than in the two other structures. Nonetheless, the number of N66-N66 hydrogen bonds in the system is 169, lower than that for the neat PNP, and only slightly higher than for the complexes containing the β-hairpin isomers. Thus, despite the possible adjustment of the peptide to the PNP through template effects, a significant change in the nanostructure of the PNP can be surmised.

In agreement with the structural features above, the $\Delta E_{reorg}^{plastic}$ values are very high for all three strutures, highest for the complex with the β-hairpin, and lowest for the one with the unordered peptide (Table 1). On the other hand, large ΔE_{reorg}^{pep} was found to be high for the unordered structure, and lower for the other two (Table 1). Since the simulations with the α-helix and β-hairpin foldamers of the peptide were conducted with constraining the geometry of the peptides, these findings make sense: The SA with these two structures did not allow any rearrangement of the peptide, resulting in low ΔE_{reorg}^{pep} data, and therefore the N66 PNP had to adjust its structure to maximize the PNP-peptide interactions. The lack of constraints with the unordered peptide allowed the oligoalanine to adjust its geometry to the N66, so $\Delta E_{reorg}^{plastic}$ became lower, and ΔE_{reorg}^{pep} became higher. These two reorganization

energies compensate each other and their sum varies in a ca. 80 kJ mol^{-1} range in the gas phase, and an even lower, 40 kJ mol^{-1} range in aqueous solution.

Despite the similarities in the reorganization energies, the ΔE_{int} differ greatly: While it is -445.0 and -492.3 kJ mol^{-1} for the α-helix and the β-hairpin, respectively, it is -800.4 kJ mol^{-1} for the unordered structure (Table 1). As a result, the adsorption energies ΔE_{ads} are positive values for the first two structures, and very negative for the latter. This means that while the adsorption of the peptide in its unordered foldamers is highly exothermic, for the other two structures it is thermodynamically unfavorable. These results show that beyond the mere number of the hydrogen bonds, other structural features, such as hydrophobic interactions,[73,74] also influence the thermodynamics of the adsorption of peptides onto N66 PNPs. The ability of the peptide to change its conformation, and adjust it to the template formed by the hydrogen bonding network of the N66 PNP is apparently a key factor, which does not only facilitate the adsorption, but this is the very effect that makes it thermodynamically feasible through the resulting higher ΔE_{int}.

These trends in ΔE_{ads} have, of course, an effect also on the relative energies of the conformations in the presence of the N66 PNP. The calculations indicate that despite the higher number of hydrogen bonds between the plastic and the peptide for the β-hairpin, the helical conformation is still more stable, and the energy difference is higher than that for the free peptide in the gas phase. Considering the aqueous solvent around the plastic-peptide associate, however, decreases the energy difference. In fact, in aqueous solution, the relative energy of the β-hairpin is by 60 kJ mol^{-1} lower than in the absence of the plastic. Although the adsorption of the peptide onto the plastic is thermodynamically unfavorable, this information is very important, since through the introduction of other amino acids — e.g. more hydrophobic ones — into the peptide, the adsorption energies might become negative. In that case, there is a further consideration that must be emphasized. The helix propensity of alanine is the highest among the amino acids,[75] and although the present peptide is relatively short, its stability in the helical conformation is considerable. Thus, for helices composed of other amino acids, the stabilization effect of the nylon in aqueous solutions on the β-conformers could mean that it is stabilized over the α-helix, providing a driving force for a

conformational change. The importance of this issue is — as indicated in the introduction — that such α-to-β structural transformations of certain proteins in the human body may result in severe health conditions.[39–41]

The effect of the PNP on the peptide structure is more severe when considering the unordered structures, which exhibit very high stabilities, with lower energies than the most stable of the structures with the α-helix isomer. The relative energy of these foldamers is somewhat decreased in the presence of water, but the $\Delta E_{rel} = -256.4$ kJ mol^{-1} is still substantial (Table 1). According to these data, the present peptide should undergo a spontaneous conformation change from the helical structure to an open-chain peptide upon adsorption onto N66 PNPs. As seen from the data above, this feature can be explained through template effects.[76,77] The exquisite stability of the open-chain unordered peptide indicates that if N66 PNP (nanoplastic) pollutants are present in the solution, peptides can lose their secondary structure entirely, and become denaturated.

4 Conclusions

Simulated annealing molecular dynamics, and quantum chemical GFN2-xTB geometry optimizations were employed to quantify the effects of nanoplastics on the folding of a small model peptide. Simulated annealing molecular dynamics was investigated in detail for the folding of two plastic nanoparticles, composed of polyethylene and nylon 6,6 with a diameter of ca. 5 nm. The settings for the folding procedure were optimized for each cases. It was found that the temperature range, in which the simulated annealing should be performed for maximal efficiency is roughly between the condensation and freezing temperature of the particle. For the estimation of these properties simple quantities were defined, which will facilitate later studies on nanoplastics.

Folding the polymer chains and the peptide together was performed in three setups, with 50 simulated annealing process for each. In the first two, the conformation of the oligoalanine peptide was constrained in a manner that it represented either an α-helix, or a β-hairpin

structure. In the third group, the conformation of the peptide was allowed to change, enabling the adaptation of the peptide conformation to the plastic. On the obtained altogether 300 structures geometry optimizations were performed with the OPLS-AA force field, and then with the quantum chemical GFN2-xTB method.

Although the α-helix of the oligoalanine is more stable than any other conformations already in the absence of the plastic, in the presence of the polyethylene nanoplastic particle the relative stability of this foldamer is increased by ca. 60 kJ mol^{-1}. For proteins composed of amino acids with a somewhat lower helix propensity than alanine, such a shift in relative energies may result in severe changes in the secondary structure. In the most stable conformation of the plastic-peptide complex the polyethylene chains surround the α-helix, suggesting that the absorption of the peptide into the plastic occurs. The other isomers of the peptide do not exhibit such behavior, showing that this process is somewhat selective. The (selective) absorption of proteins into plastic particles can apply a certain strain on the biomolecule, affecting its structure.

The nylon nanoparticle shows a high degree of order in its structure, with long chains of hydrogen bonding amide moieties, ordered parallel to each other, separating polar and nonpolar domains within the nanoplastic particle. This suggests that nylon 6,6 nanoplastics are self-organizing materials. The presence of the peptide was found to perturb this microstructure, which destabilized complexes with α-helical and β-hairpin foldamers of the peptide. On the other hand, through assuming an unordered open-chain conformation, the peptide can maximize its interactions with the template formed by the highly ordered nylon 6,6 surface. Consequently, the adsorption of the oligoalanine onto the nylon 6,6 particle is exothermic, whereas that of the other two isomers is thermodynamically hindered, which suggests that proteins would fully lose their characteristic secondary structure, and would denaturate upon contact with this kind of nanoplastics.

Based on the results above multiple, practically relevant observations can be made. First of all, modeling and theory in general, and the simulated annealing approach in particular revealed important structural information on these systems, and can be thereby considered a powerful asset in nanoplastic research. Both plastics were found to influence the relative sta-

bility of characterstic secondary structures of the model peptide. Since such conformational changes of proteins can severely affect human health, considering that plastics can enter the organs and the blood of organisms,[33] these results highlight the importance of further research in the field. Moreover, the effects of the two plastics investigated here were very different on the peptide structure, supporting earlier assumptions[27] that using polystyrene nanoparticles as a general model for nanoplastics is erroneous.

Acknowledgment

The technical help of Sebastian Ehlert with the XTB program is greatfully acknowledged.

References

[1] Carpenter, E. J.; Anderson, S. J.; Harvey, G. R.; Miklas, H. P.; Peck, B. B. *Science* **1972,** *178,* 749–750.

[2] Ryan, P. G.; Moore, C. J.; van Franeker, J. A.; Moloney, C. L. *Philos. Trans. R. Soc. B* **2009,** *364,* 1999–2012.

[3] Ryan, P. G.; Moloney, C. L. *Nature* **1993,** *361,* 23.

[4] Law, K. L.; Thompson, R. C. *Science* **2014,** *345,* 144–145.

[5] Thompson, R. C.; Olsen, Y.; Mitchell, R. P.; Davis, A.; Rowland, S. J.; John, A. W.; McGonigle, D.; Russell, A. E. *Science* **2004,** *304,* 838–838.

[6] Li, J.; Qu, X.; Su, L.; Zhang, W.; Yang, D.; Kolandhasamy, P.; Li, D.; Shi, H. *Environ. Pollut.* **2016,** *214,* 177–184.

[7] Bellas, J.; Martínez-Armental, J.; Martínez-Cámara, A.; Besada, V.; Martínez-Gómez, C. *Mar. Pollut. Bull.* **2016,** *109,* 55–60.

[8] Collard, F.; Gilbert, B.; Eppe, G.; Parmentier, E.; Das, K. *Arch. Environ. Contam. Toxicol.* **2015,** *69,* 331–339.

[9] Lusher, A.; Mchugh, M.; Thompson, R. *Mar. Pollut. Bull.* **2013,** *67,* 94–99.

[10] Lusher, A. L.; Hernandez-Milian, G.; O'Brien, J.; Berrow, S.; O'Connor, I.; Officer, R. *Environ. Pollut.* **2015,** *199,* 185–191.

[11] Kim, J.-S.; Lee, H.-J.; Kim, S.-K.; Kim, H.-J. *Environ. Sci. Technol.* **2018,** *52,* 12819–12828.

[12] Alimi, O. S.; Farner Budarz, J.; Hernandez, L. M.; Tufenkji, N. *Environ. Sci. Technol.* **2018,** *52,* 1704–1724.

[13] Oriekhova, O.; Stoll, S. *Environ. Sci. Nano* **2018,** *5,* 792–799.

[14] Bordós, G.; Urbányi, B.; Micsinai, A.; Kriszt, B.; Palotai, Z.; Szabó, I.; Hantosi, Z.; Szoboszlay, S. *Chemosphere* **2019,** *216,* 110–116.

[15] Al-Jaibachi, R.; Cuthbert, R. N.; Callaghan, A. *Biol. Lett.* **2018,** *14,* 20180479.

[16] Mitrano, D. *Nat. Nanotechnol.* **2019,** *14,* 299.

[17] Boots, B.; Russel, C. W.; Green, D. S. *Environ. Sci. Technol.* **2019,** *53,*.

[18] Rowenczyk, L. *et al. Environ. Sci. Technol.* **2020,** *54,* 4102–4109.

[19] Bi, M.; He, Q.; Chen, Y. **2020,** doi: 10.1021/acs.est.0c01009.

[20] Lozano, Y. M.; Rillig, M. C. *Environ. Sci. Technol.* **2020,** doi: 10.1021/acs.est.0c01051.

[21] Foekema, E. M.; De Gruijter, C.; Mergia, M. T.; van Franeker, J. A.; Murk, A. J.; Koelmans, A. A. *Environ. Sci. Technol.* **2013,** *47,* 8818–8824.

[22] Cox, K. D.; Covernton, G. A.; Davies, H. L.; Dower, J. F.; Juanes, F.; Dudas, S. E. *Environ. Sci. Technol.* **2019,** *53,* 7068–7074.

[23] Zhang, Q.; Xu, E. G.; Li, J.; Chen, Q.; Ma, L.; Zeng, E. Y.; Shi, H. *Environ. Sci. Technol.* doi: 10.1021/acs.est.9b04535.

[24] Smith, M.; Love, D. C.; Rochman, C. M.; Neff, R. A. *Curr. Environ. Health Rep.* **2018,** *5,* 375–386.

[25] Sedlak, D. *Environ. Sci. Technol.* **2017,** *51,*.

[26] Burton, G. A. *Environ. Sci. Technol.* **2017,** *51,* 13515-13516.

[27] Koelmans, A. A.; Besseling, E.; Shim, W. J. Nanoplastics in the aquatic environment. Critical review. In *Marine anthropogenic litter*; Springer, Cham: 2015.

[28] McNeish, R.; Kim, L.; Barrett, H.; Mason, S.; Kelly, J.; Hoellein, T. *Sci. Rep.* **2018,** *8,* 11639.

[29] Sussarellu, R. *et al. Proc. Natl. Acad. Sci.* **2016,** *113,* 2430–2435.

[30] Lamb, J. B. *et al. Science* **2018,** *359,* 460–462.

[31] Rist, S.; Almroth, B. C.; Hartmann, N. B.; Karlsson, T. M. *Sci. Tot. Environ.* **2018,** *626,* 720–726.

[32] Lenz, R.; Enders, K.; Nielsen, T. G. *Proc. Natl. Acad. Sci.* **2016,** *113,* E4121–E4122.

[33] Al-Sid-Cheikh, M.; Rowland, S. J.; Stevenson, K.; Rouleau, C.; Henry, T. B.; Thompson, R. C. *Environ. Sci. Technol.* **2018,** *52,* 14480–14486.

[34] Huffer, T.; Praetorius, A.; Wagner, S.; von der Kammer, F.; Hofmann, T. *Environ. Sci. Technol.* **2017,** *51,*.

[35] Syberg, K.; Khan, F. R.; Selck, H.; Palmqvist, A.; Banta, G. T.; Daley, J.; Sano, L.; Duhaime, M. B. *Environ. Toxicol. Chem.* **2015,** *34,* 945–953.

[36] Bochicchio, D.; Panizon, E.; Monticelli, L.; Rossi, G. *Sci. Rep.* **2017,** *7,* 6357.

[37] Hollóczki, O.; Gehrke, S. *ChemPhysChem* **2020,** *21,* 9–12.

[38] Hollóczki, O.; Gehrke, S. *Sci. Rep.* **2019,** *9,* 16013.

[39] Hegde, R. S.; Mastrianni, J. A.; Scott, M. R.; DeFea, K. A.; Tremblay, P.; Torchia, M.; DeArmond, S. J.; Prusiner, S. B.; Lingappa, V. R. *Science* **1998,** *279,* 827–834.

[40] Saborio, G. P.; Permanne, B.; Soto, C. *Nature* **2001,** *411,* 810–813.

[41] Kirschner, D. A.; Abraham, C.; Selkoe, D. J. *Proc. Natl. Acad. Sci.* **1986,** *83,* 503–507.

[42] Ding, J.; Huang, Y.; Liu, S.; Zhang, S.; Zou, H.; Wang, Z.; Zhu, W.; Geng, J. *J. Hazard. Mater.* **2020,** 122693.

[43] Gopinath, P. M.; Saranya, V.; Vijayakumar, S.; Meera, M. M.; Ruprekha, S.; Kunal, R.; Pranay, A.; Thomas, J.; Mukherjee, A.; Chandrasekaran, N. *Sci. Rep.* **2019,** *9,* 8860.

[44] Kihara, S.; van der Heijden, N. J.; Seal, C. K.; Mata, J. P.; Whitten, A. E.; Koper, I.; McGillivray, D. J. *Bioconjugate Chem.* **2019,** *30,* 1067–1076.

[45] Christ, C. D.; van Gunsteren, W. F. *J. Chem. Phys.* **2007,** *126,* 184110.

[46] Christ, C. D.; Mark, A. E.; Van Gunsteren, W. F. *J. Comput. Chem.* **2010,** *31,* 1569–1582.

[47] Zhang, C.; Ma, J. *J. Chem. Phys.* **2010,** *132,* 244101.

[48] Elber, R.; Karplus, M. *J. Am. Chem. Soc.* **1990,** *112,* 9161–9175.

[49] Kukharenko, O.; Sawade, K.; Steuer, J.; Peter, C. *J. Chem. Theor. Comput.* **2016,** *12,* 4726–4734.

[50] Lemke, T.; Peter, C.; Kukharenko, O. *J. Chem. Comput. Theor.* **2018,** *14,* 5476–5488.

[51] Affentranger, R.; Tavernelli, I.; Di Iorio, E. E. *J. Chem. Theor. Comput.* **2006,** *2,* 217–228.

[52] Sugita, Y.; Okamoto, Y. *Chem. Phys. Lett.* **1999,** *314,* 141–151.

[53] Abrams, C.; Bussi, G. *Entropy* **2014,** *16,* 163–199.

[54] Barducci, A.; Bonomi, M.; Parrinello, M. *WIREs: Comp. Mol. Sci.* **2011,** *1,* 826–843.

[55] Bussi, G.; Laio, A. *Nat. Rev. Phys.* **2020,** *2,* 200–212.

[56] Wille, L. *Chem. Phys. Lett.* **1987,** *133,* 405–410.

[57] Wilson, S. R.; Cui, W.; Moskowitz, J. W.; Schmidt, K. E. *Tetrahedron Lett.* **1988,** *29,* 4373–4376.

[58] Wilson, S. R.; Cui, W. *Biopolymers: Original Research on Biomolecules* **1990,** *29,* 225–235.

[59] Laughton, C. *Protein Eng. Des. Sel.* **1994,** *7,* 235–241.

[60] Hao, G.-F.; Xu, W.-F.; Yang, S.-G.; Yang, G.-F. *Sci. Rep.* **2015,** *5,* 15568.

[61] Hatmal, M. M.; Taha, M. O. *Future Med. Chem.* **2017,** *9,* 1141–1159.

[62] Dawson, A. L.; Kawaguchi, S.; King, C. K.; Townsend, K. A.; King, R.; Huston, W. M.; Bengtson Nash, S. M. *Nat. Commun.* **2018,** *9,* 1001.

[63] Plimpton, S. *J. Comp. Phys.* **1995,** *117,* 1–19 http://lammps.sandia.gov.

[64] Jorgensen, W. L.; Maxwell, D. S.; Tirado-Rives, J. *J. Am. Chem. Soc.* **1996,** *118,* 11225–11236.

[65] Brehm, M.; Kirchner, B. *J. Chem Inf. Model.* **2011,** *51,* 2007–2023.

[66] Brehm, M.; Thomas, M.; Gehrke, S.; Kirchner, B. *J. Chem. Phys.* **2020,** *152,* 164105.

[67] Grimme, S.; Bannwarth, C.; Shushkov, P. *J. Chem. Theor. Comput.* **2017,** *13,* 1989–2009.

[68] Bannwarth, C.; Ehlert, S.; Grimme, S. *J. Chem. Theor. Comput.* **2019,** *15,* 1652–1671.

[69] Caldeweyher, E.; Bannwarth, C.; Grimme, S. *J. Chem. Phys.* **2017,** *147,* 034112.

[70] Caldeweyher, E.; Ehlert, S.; Hansen, A.; Neugebauer, H.; Spicher, S.; Bannwarth, C.; Grimme, S. *J. Chem. Phys.* **2019,** *150,* 154122.

[71] Schmitz, S.; Seibert, J.; Ostermeir, K.; Hansen, A.; Göller, A. H.; Grimme, S. *J. Phys. Chem. B* **2020,** .

[72] Cochran, A. G.; Skelton, N. J.; Starovasnik, M. A. *Proc. Natl. Acad. Sci.* **2001,** *98,* 5578–5583.

[73] McCrea-Hendrick, M. L.; Bursch, M.; Gullett, K. L.; Maurer, L. R.; Fettinger, J. C.; Grimme, S.; Power, P. P. *Organometallics* **2018,** *37,* 2075–2085.

[74] Bursch, M.; Caldeweyher, E.; Hansen, A.; Neugebauer, H.; Ehlert, S.; Grimme, S. *Acc. Chem. Res.* **2018,** *52,* 258–266.

[75] Pace, C. N.; Scholtz, J. M. *Biophys. J.* **1998,** *75,* 422–427.

[76] Elfgen, R.; Hollóczki, O.; Kirchner, B. *Acc. Chem. Res.* **2017,** *50,* 2949–2957.

[77] Steed, J. W.; Atwood, J. L. *Supramolecular chemistry;* John Wiley & Sons: 2013.